

Exciton Interactions in Helical Crystals of a Hydrogen-Bonded Eumelanin Monomer

Devika Sasikumar, Kavya Vinod, Jeswin Sunny and Mahesh Hariharan*^a

^aSchool of Chemistry, Indian Institute of Science Education and Research Thiruvananthapuram, Vithura, Thiruvananthapuram, Kerala, India 695551

Supporting Information (SI) Contents

Section A: Syntheses and Characterization	S3
Section B: Materials and Methods	S4
Section C: Tables	
Table S1: Crystallographic data and refinement parameters for DHI monomer	S6
Table S2: Relative % of intermolecular interactions obtained from Hirshfeld analysis.....	S6
Table S3: NICS(1) values calculated for the various dimers in DHI crystal.....	S7
Table S4. Interaction energies ^[a] of DHI dimers evaluated using symmetry-adapted perturbation theory (SAPT(0)) aug-cc-pVDZ calculations.....	S7
Table S5. Energy (ΔE), oscillator strength (f), mean position (POS), participation ratio (PR) of initial orbital (hole) and final orbital (electron) and charge transfer character (CT) of excited singlet states in D1.....	S7
Table S6. Energy (ΔE), oscillator strength (f), mean position (POS), participation ratio (PR) of initial orbital (hole) and final orbital (electron) and charge transfer character (CT) of excited singlet states in D2.....	S8
Table S7. Energy (ΔE), oscillator strength (f), mean position (POS), participation ratio (PR) of initial orbital (hole) and final orbital (electron) and charge transfer character (CT) of excited singlet states in D3.....	S8
Table S8. Energy (ΔE), oscillator strength (f), mean position (POS), participation ratio (PR) of initial orbital (hole) and final orbital (electron) and charge transfer character (CT) of excited singlet states in D4.....	S8
Table S9. Photophysical properties of DHI monomer in different solvents.....	S9
Section D. Figures	
Figure S1: Optical Microscope Images of a) DHI crystal, b)-f) Microcrystalline aggregates of DHI trimer.....	S10

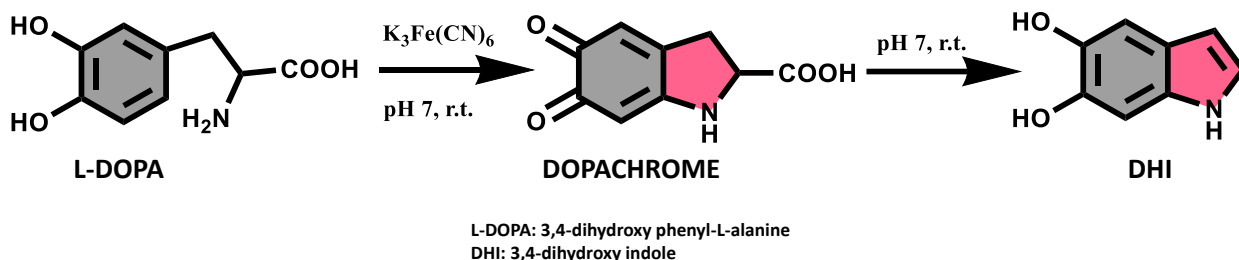
Figure S2: a-b) The enantiomeric zig-zag helical stacks in the DHI crystal. The zig-zag helical stacks proceeding along the crystallographic c) a-axis and d) c-axis where each colour represents the adjacent enantiomeric stacks.	S10
Figure S3: Hirshfeld surface analysis of DHI crystal.....	S11
Figure S4: QTAIM electron density map showing the synthon formation from hydrogen bonding interactions in a) D1, b) D2, c) D3 and d) D4.	S11
Figure S5: A and B molecules for NICS(1) calculation in dimers (a) D1, (b) D2, (c) D3, (d) D4.....	S12
Figure S6: Powder-XRD pattern for DHI crystal and DHI-T	S12
Figure S7: a) Molecular structure predicted for DHI trimer (DHI-T), b) Optimized structure of DHI-T at CAM-B3LYP/6-311g+(d,p) level of theory.....	S12
Figure S8: (a) Normalized absorption and (b) fluorescence emission profiles of monomeric DHI in various solvents.....	S13
Figure S9: UV-vis absorption (grey) and normalized fluorescence emission (red) profiles of monomeric DHI in CHCl ₃	S13
Figure S10: (a) Normalized absorption and fluorescence emission profiles for DHI crystal	S13
Figure S11: Shows (a) concurrent CD and (b) LD spectra obtained for the bulk DHI crystal collected on different days, each with freshly crystallized samples at varied concentration ratio of sample:KBr. c) Kubelka-Munk diffuse reflectance spectrum (bottom) and CD spectrum (top) of DHI crystal with the zero crossing at ~371 nm.	S14
Section E. Appendix: Characterisation Data	
Appendix C1. HRMS Spectrum for DHI monomer.....	S15
Appendix C2: ¹ H-NMR Spectrum of DHI in CDCl ₃	S15
Appendix C3: ¹ H-NMR Spectrum of DHI in DMSO-d ₆	S16
Appendix C4: ¹³ C-NMR Spectrum of DHI in DMSO-d ₆	S16
Appendix C5: MALDI-MS Spectra of DHI-oligomer dissolved in a) CHCl ₃ and b) DMSO	S17
Appendix C6: ¹ H-NMR spectrum showing the presence of DHI-T in aggregate concentrations of DHI in CDCl ₃	S17
Appendix C7: IR Spectrum of DHI in a) KBr pellet and b) chloroform solution	S18
Appendix C8: IR Spectrum of DHI-T in KBr pellet	S18
Appendix C9: Shows the overlapped 2D ¹ H-COSY (red) and -NOESY (blue) NMR spectra of DHI in CDCl ₃	S19
Section F:	
References.....	S20

Section A: Syntheses and Characterization

All chemicals were obtained from commercial suppliers and used as received without further purification. All reactions were carried out in oven-dried glassware prior to use and wherever necessary, were performed under dry nitrogen in distilled solvents using standard gastight syringes, cannula, and septa. Solvents used for characterization were dried and distilled by standard laboratory purification techniques. Yields refer to spectroscopically homogenous substances. Melting points were obtained using a capillary melting point apparatus. ^1H and ^{13}C NMR spectra was measured on a 500 MHz Bruker Advance DPX spectrometer. Internal standard used for ^1H NMR and ^{13}C NMR is 1,1,1,1-tetramethyl silane (TMS). High resolution mass spectra (HRMS) were recorded on Thermo Scientific Q Exactive Mass Spectrometer using Electrospray Ionization (ESI) technique. MALDI-TOF Mass Spectra were recorded on Bruker UltraFlex extreme MALDI-TOF mass spectrometer by directly ionizing the sample without using a matrix. IR spectra were recorded on a Shimadzu IR Prestige-21 FT-IR spectrometer with KBr pellets. Photophysical measurements of the derivatives were carried out in a cuvette of 3 mm path length. Absorption and emission spectra were recorded on Shimadzu UV-3600 UV-VIS-NIR and Horiba Jobin Yvon Fluorolog spectrometers, respectively. The Kubelka-Munk transformed reflectance spectra in the crystalline state were measured in the diffuse reflectance mode. CD spectrum of samples in solid state were recorded in circular dichroism spectrometer MOS500 supplied by BioLogic Science Instrument. For obtaining solid state CD spectrum, KBr was powdered and dried in vacuum oven at 80°C for 3 h. A transparent KBr pellet was used for recording a baseline. Transparent pellets of samples were made by pressing a mixture of 1:100 sample:KBr and the measurement was done immediately. Powder X-ray diffraction (PXRD) spectra were recorded using an X'pert PRO (PANalytics) powder diffractometer with Cu as the anode material ($K\alpha_1 = 1.54 \text{ \AA}$). The optical microscopic images were recorded on Olympus SZX-2-ILLB Trinocular Stereomicroscope with Digital Camera. Lifetime measurements were carried out in an IBH picosecond time-correlated single-photon counting (TCSPC) system. The pulse width of the excitation ($\lambda_{\text{exci}} = 310 \text{ nm}$) source is determined to be $<100 \text{ ps}$ and the fluorescence decay profiles were de-convoluted using DAS6.3 and fitted with exponential decay, minimizing the χ^2 values.

Synthesis of DHI:

The synthesis procedure follows the reported literature with minor modifications.¹ A solution of 1g (5 mmol) L-dopa in water (500 ml) and a solution of $\text{K}_3[\text{Fe}(\text{CN})_6]$ (6.6 g, 20 mmol) and NaHCO_3 (2.5 g, 30 mmol) in water (60 ml) were separately degassed by purging with an argon flux for 10 min. The solution of $\text{K}_3[\text{Fe}(\text{CN})_6]$ and NaHCO_3 was poured at once to the solution of dopa while vigorous stirring at room temperature. L-dopa upon chemical oxidation using potassium ferricyanide turns into a wine-red solution of dopachrome. Dopachrome further undergoes decarboxylation at room temperature to yield white amorphous powders of 5,6-dihydroxyindole (DHI). The reaction is maintained in a weakly basic medium that facilitates an oxidative nucleophilic reaction followed by the cyclisation of L-dopa. Solid $\text{Na}_2\text{S}_2\text{O}_5$ (5.0 g, 26 mmol) was then added to the dark brown solution, which was extracted with ethyl acetate (300 ml x 3). The ethyl acetate extracts were combined, washed once with saturated NaCl solution (100 ml), and dried over anhydrous Na_2SO_4 (50 g). Evaporation of ethyl acetate gave a brown oil to which a solution of hexane (20 ml) was added to give almost white powders of DHI. Several preparations gave yields of 61-64% (in the literature, the yield was 40%).



Scheme S1: Shows the reaction scheme for the synthesis of DHI.

¹H NMR (500 MHz, CDCl₃, ppm): δ = 7.85 (s, 1H), 7.01 (t, J = 3 Hz, 2H), 6.86 (s, 1H), 6.32 (s, 1H), 5.29 (s, 1H), 4.89 (s, 1H).

¹³C NMR (125 MHz, DMSO-d₆, ppm): δ = 142.91, 140.81, 130.70, 123.04, 120.70, 104.89, 100.62, 97.59.

M.P.: 170°C

HRMS (ESI) (m/z): Calculated for C₈H₇NO₂: 149.0477, found: 150.0550 [M+H]⁺

IR (cm⁻¹): 3437.15 (broad); 1631.78; 1473.62 (s); 1415.75 (s)

Section B: Materials and Methods

X-ray Crystallography: High quality single crystals of DHI were used for X-ray diffraction experiments. Single crystal was mounted using oil (Infineum V8512) on a glass fiber. All measurements were made on a CCD area detector with graphite monochromated Mo K α radiation. The data was collected using Bruker APEXII detector and processed using APEX2 from Bruker. The structure was solved by direct method and expanded using Fourier technique. The non-hydrogen atoms were refined anisotropically. Hydrogen atoms were included in idealized positions, but not refined. Their positions were constrained relative to their parent atom using the appropriate HFIX command in SHELX-97.² All programs used during the crystal structure analysis are incorporated in the WINGX software.³ The full validation of CIF and structure factor of DHI was performed using the checkCIF utility and found to be free of major alert levels. Three-dimensional structure visualization and the exploration of the crystal packing of crystals under study were carried out using Mercury 3.5.1.⁴

Computational Methods: Single point energy and dipole moments were calculated at the CAM-B3LYP/6-311g+(d,p) level of theory. All these computations were performed using the Gaussian 16 suite.⁵

Quantum Theory of Atoms in Molecules (QTAIM):⁶ The wave function generation for the DHI dimer orientations were carried out at CAM-B3LYP/6-311g+(d,p) level of theory using Gaussian16. Quantum theory of atoms in molecules (QTAIM) analyses helps to understand the description of interatomic interaction in the single crystal X-ray structure. A bond is defined along the bond line between two nuclei, called a bond path, along which electron density is concentrated. The (3, -1) bond critical point (BCP) is a point along the bond path at the interatomic surface, where the shared electron density reaches a minimum. (3, +1) ring critical point (RCP) and (3, +3) cage critical point (CCP) represents critical points in the ring and cage respectively where the electron density is minimum. The physical characteristics of the critical points [the electron density at BCP, RCP and CCP, $\rho(r)$, and its Laplacian, $\nabla^2\rho(r)$ reveal the

approximate measure of the amount of electron density built up in the bonding region and as such could be taken as characteristic of the bond. When $\nabla^2\rho(r)<0$ and is large in magnitude, $\rho(r)$ is also large which means that there is a concentration of electronic charge in the internuclear region. This is also an indication of a sharing of electronic charge between both nuclei that defines the covalent (polar) bond. When $\nabla^2\rho(r)>0$ there is a depletion of electronic charge in the internuclear region and it indicates a closed shell interaction. Using the AIMAIL software package, the electron density was integrated over atomic basins according to the quantum theory of atoms in molecules using PROAIM, and thus the BCP, RCP, CCP data and the molecular graphs were obtained.

Hirshfeld Analysis:⁷ Important intermolecular interactions within the structure of DHI were identified through Hirshfeld surface analysis using CrystalExplorer17. The Hirshfeld surface is defined as a set of points in 3D space where the ratio of promolecule and procrystal electron densities is equal to 0.5. The exploration of intermolecular contacts is provided by mapping normalized contact distances (d_{norm}), which is a function of a closest distance from the point to the nuclei interior (d_i) and exterior (d_e) to the surface as well as on the van der Waals radii (r_{vdw}). 2D fingerprint plots derived from the Hirshfeld surface analyses, by plotting the fraction of points on the surface as the function of d_i and d_e , provides a visual summary of intermolecular contacts within the crystal.

TheoDRE Analysis:^{8,9} The excitations of DHI dimers D1, D2, D3 and D4 at the DFT optimized structure were analyzed using TheoDRE.^{7,8} The parameters used to investigate the excited state characteristics are participation ratio (PR), mean position (POS) of initial orbital (hole) and final orbital (electron), and charge transfer character (CT). The magnitude of PR relates to the number of fragments participating in the excitation; hence, in our investigation, the PR ranges from 1 to 2. POS provides the mean position of hole and electron for a particular excitation. Charge transfer states and delocalized Frenkel states show POS = 1.5. If the Frenkel state is localized on monomer A, then POS = 1, and if localized on monomer B, POS = 2, for a dimer AB. Finally, CT is related to the total weight of configurations where initial and final orbitals are situated on different fragments. A CT value of 1 denotes the presence of a charge-separated state, and CT = 0 refers to Frenkel states.

Symmetry Adapted Perturbation Theory (SAPT):¹⁰ SAPT(0) analysis was employed to determine the non-covalent interaction energies of dimer molecules. The SAPT module of the psi4 code was employed, with jun-cc-pVDZ basis set. SAPT(0) calculations provide the contributing components of interaction energy. The results obtained from SAPT(0) analysis is a second order perturbation expansion constituting first order electrostatic and exchange energy parts and second order dispersion, induction and their exchange counterparts as the perturbation terms.

$$E_{\text{int}}^{\text{SAPT}(0)} = E_{\text{elc}}^{(1)} + E_{\text{ex}}^{(1)} + E_{\text{ind}}^{(2)} + E_{\text{ind-ex}}^{(2)} + E_{\text{dis}}^{(2)} + E_{\text{dis-ex}}^{(2)}$$

Section C: Tables

Table S1. Crystallographic data and refinement parameters for DHI monomer

Parameters	DHI
Formula	C ₈ H ₇ NO ₂
Formula weight	149.15
Color	Colorless
Crystal system	Orthorhombic
Space group, Z	<i>P</i> 2 ₁ 2 ₁ 2 ₁ , 4
a (Å)	5.862
b (Å)	7.712
c (Å)	14.907
α, deg	90
β, deg	90
γ, deg	90
Volume, Å ³	673.9
R factor	4.71
Temp, K	296
d _{calculated} (mg/m ³)	1.470
No. of reflections collected	5841
No. of unique reflections	1183
2θ _{max} , deg	24.995
No. of parameters	102
R1, wR2, (I > 2s(I))	0.0689, 0.1155
R1, wR2 (all data)	0.0471, 0.1044
Goodness of fit	1.023
CCDC number	2120651

Table S2. Relative % intermolecular interactions obtained from Hirshfeld analysis.

Interaction (%)	C...H	H...H	N...H	O...H
DHI	40.5	29.7	4.3	25.4

Table S3. NICS(1) values calculated for the various dimers in DHI crystal.

Monomer	6C		5C	
	-26.14		-28.03	
Dimer	Molecule A #		Molecule B #	
	6C	5C	6C	5C
D1	-27.22	-29.13	-25.56	-27.63
D2	-26.41	-28.39	-29.43	-31.48
D3	-25.47	-27.57	-25.92	-27.92
D4	-25.61	-26.76	-25.42	-27.77

The molecules represented as A and B are shown in Figure S5

Table S4. Interaction energies^[a] of DHI dimers evaluated using symmetry-adapted perturbation theory (SAPT(0)) aug-cc-pVDZ calculations.

Dimer	SAPT(0) E_{int}^{SAPT}	Electrostatic energy $E_{elc}^{(1)}$	Dispersion energy $E_{dis}^{(2)}$	Induction energy $E_{ind}^{(2)}$	Exchange energy $E_{ex}^{(1)}$
D1	-9.70	-6.17	-8.49	-1.60	6.56
D2	-5.69	-1.67	-7.65	-0.70	4.34
D3	-6.57	-6.14	-3.51	-1.38	4.46
D4	-2.63	-1.52	-2.85	-0.70	2.45

^[a]All energy values are provided in kcal/mol

Table S5. Energy (ΔE), oscillator strength (f), mean position (POS), participation ratio (PR) of initial orbital (hole) and final orbital (electron) and charge transfer character (CT) of excited singlet states in D1.

Energy State	dE(eV)	f	POS	PR	CT
S1	4.619	0.009	1.648	1.839	0.04
S2	4.678	0.252	1.333	1.796	0.081
S3	4.877	0.03	1.586	1.357	0.698
S4	4.977	0.05	1.878	1.276	0.1
S5	5.015	0.066	1.127	1.285	0.036
S6	5.124	0.001	1.77	1.504	0.434
S7	5.316	0.004	1.837	1.39	0.285
S8	5.351	0.002	1.092	1.206	0.136
S9	5.451	0.001	1.667	1.422	0.648
S10	5.538	0.002	1.8	1.465	0.385

Table S6. Energy (ΔE), oscillator strength (f), mean position (POS), participation ratio (PR) of initial orbital (hole) and final orbital (electron) and charge transfer character (CT) of excited singlet states in D2.

State	dE(eV)	f	POS	PR	CT
S1	4.625	0.001	1.54	1.987	0.024
S2	4.689	0.282	1.453	1.982	0.021
S3	4.935	0.007	1.423	1.929	0.14
S4	4.946	0.055	1.049	1.102	0.036
S5	4.983	0.064	1.584	1.944	0.047
S6	5.131	0.005	1.895	1.24	0.175
S7	5.255	0.003	1.206	1.473	0.395
S8	5.3	0.009	1.343	1.524	0.556
S9	5.427	0.003	1.35	1.827	0.171
S10	5.45	0.001	1.656	1.823	0.188

Table S7. Energy (ΔE), oscillator strength (f), mean position (POS), participation ratio (PR) of initial orbital (hole) and final orbital (electron) and charge transfer character (CT) of excited singlet states in D3.

State	dE(eV)	f	POS	PR	CT
S1	4.769	0.223	1.061	1.13	0.005
S2	4.819	0.166	1.939	1.13	0.002
S3	5.132	0.087	1.997	1.006	0.001
S4	5.149	0.108	1.007	1.013	0.005
S5	5.792	0	1.5	1.002	0.998
S6	6.125	0.001	1.5	1.002	0.998
S7	6.247	0.001	1	1.001	0.001
S8	6.339	0.278	1.115	1.256	0.005
S9	6.348	0.247	1.879	1.27	0.004
S10	6.472	0.002	1.015	1.031	0.004

Table S8. Energy (ΔE), oscillator strength (f), mean position (POS), participation ratio (PR) of initial orbital (hole) and final orbital (electron) and charge transfer character (CT) of excited singlet states in D4.

State	dE(eV)	f	POS	PR	CT
S1	4.764	0.339	1.29	1.7	0.003
S2	4.816	0.079	1.707	1.708	0.003
S3	5.107	0.107	1.178	1.413	0.003
S4	5.121	0.045	1.825	1.406	0.002
S5	5.625	0	1.496	1.009	0.991
S6	6.053	0.004	1.151	1.364	0.301
S7	6.149	0.004	1.497	1.023	0.977
S8	6.302	0.17	1.452	1.982	0.023
S9	6.347	0.013	1.813	1.439	0.125
S10	6.365	0.31	1.59	1.936	0.02

Table S9. Photophysical properties of DHI monomer in different solvents.

Solvent	λ_{em} (nm)	Fluorescence Quantum Yield (%)	Fluorescence Emission Lifetime (ns) [Relative Amplitude in %]
Toluene	320	3.80	0.10
DCM	335	0.50	<1
THF	335	0.50	2.02
CHCl ₃	335, 460	1.20	335 nm = <1
			460 nm = 1.17 [81%] 8.60 [19%]
Ethyl Acetate	325	4.00	0.52
MeOH	331	29.00	1.75
ACN	333	15.50	2.13
Water	350	0.90	<1 [95%] 4.38 [5%]

Section D: Figures

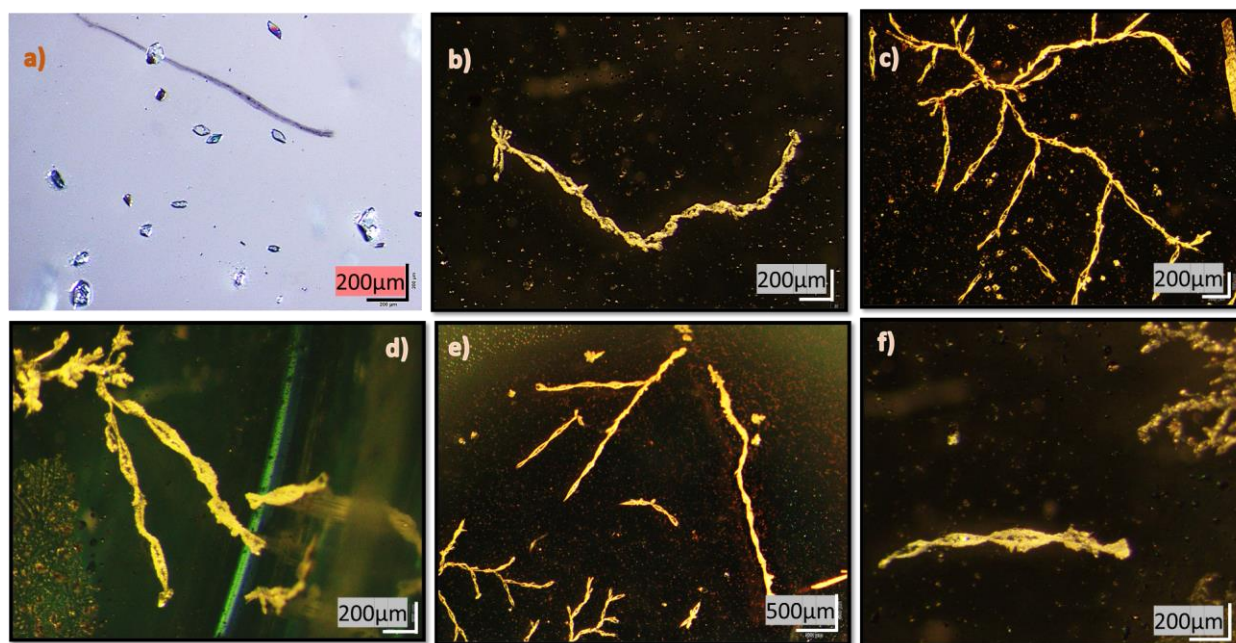


Figure S1: Optical microscope images of **a)** DHI crystal, **b)-f)** Double-helical microcrystalline aggregates of DHI trimer.

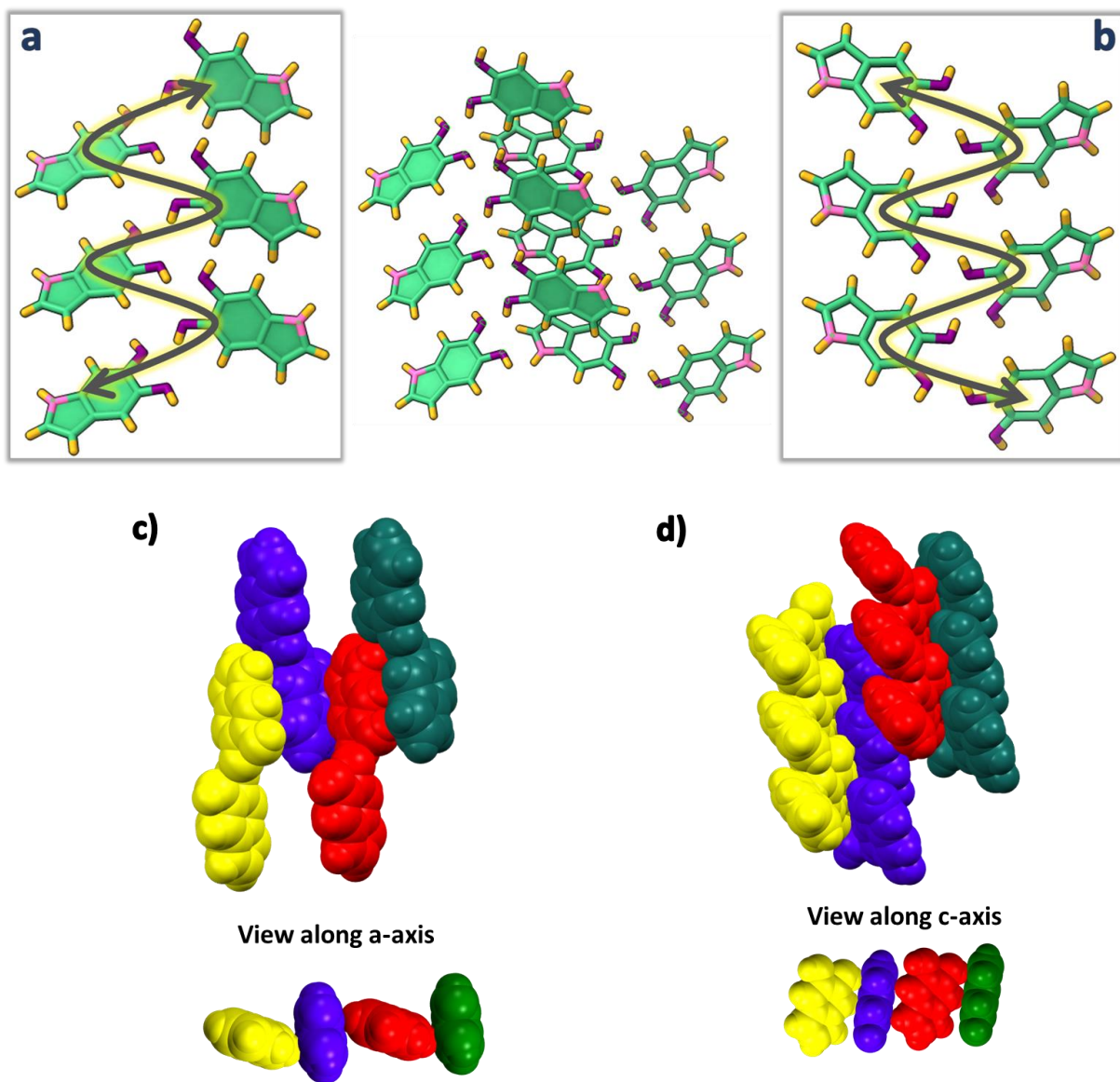


Figure S2: a-b) Shows the enantiomeric zig-zag helical stacks in the DHI crystal. The zig-zag helical stacks proceed along the crystallographic **c)** a-axis and **d)** c-axis where each colour represents the adjacent enantiomeric stacks. The enantiomeric stacks are connected in herringbone fashion as shown in (d).

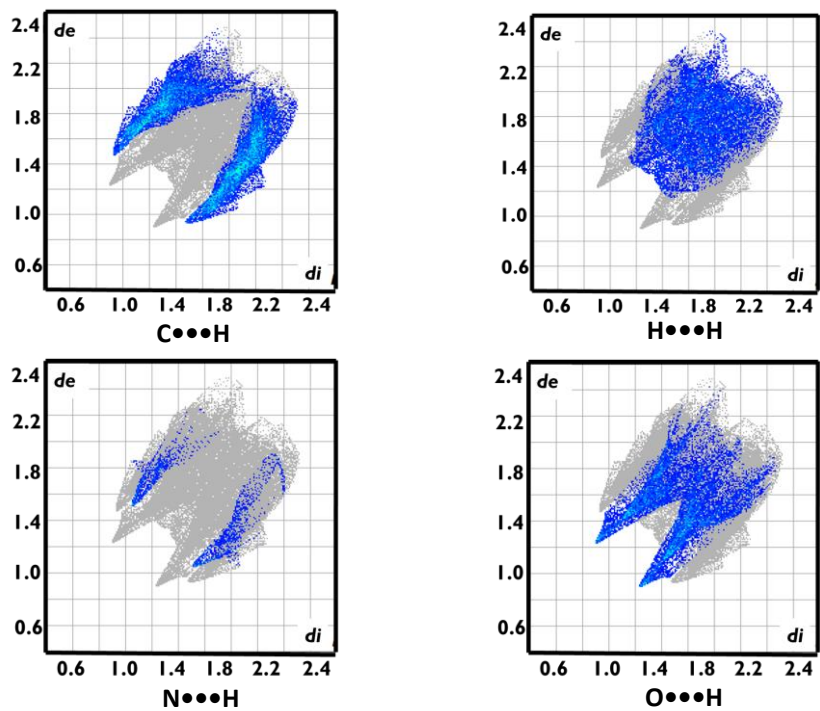


Figure S3: Hirshfeld surface analysis of DHI crystal.

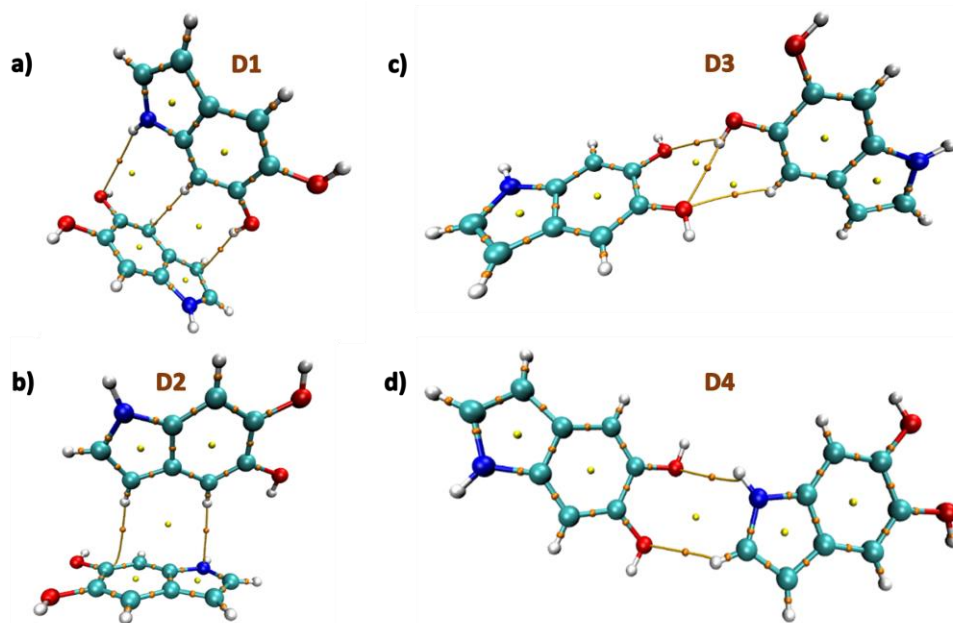


Figure S4: QTAIM electron density map showing the synthon formation from hydrogen bonding interactions in **a)** D1, **b)** D2, **c)** D3 and **d)** D4.

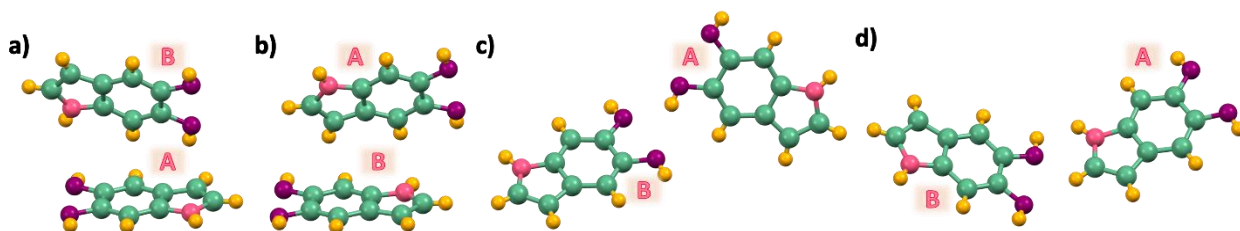


Figure S5: A and B molecules for NICS(1) calculation in dimers **a)** D1, **b)** D2, **c)** D3 and **d)** D4.

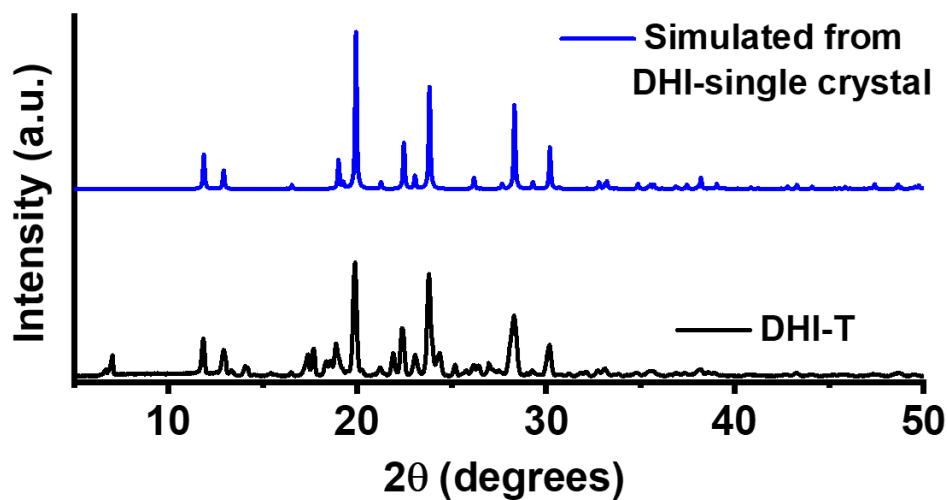


Figure S6: Powder-XRD pattern for DHI crystal and DHI-T.

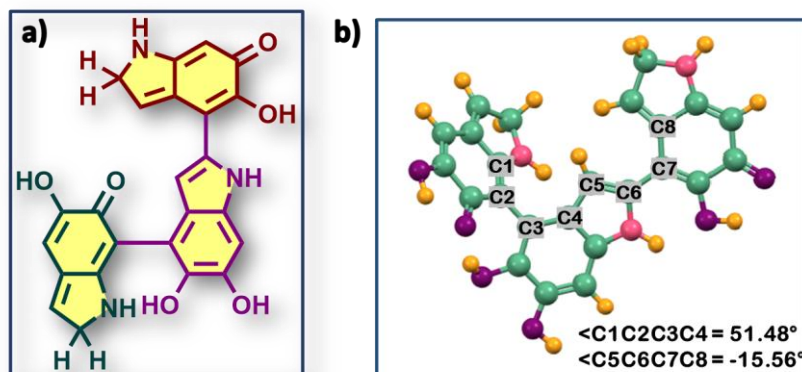


Figure S7: **a)** Molecular structure predicted for DHI trimer (DHI-T), **b)** Optimized structure of DHI-T at CAM-B3LYP/6-311g+(d,p) level of theory.

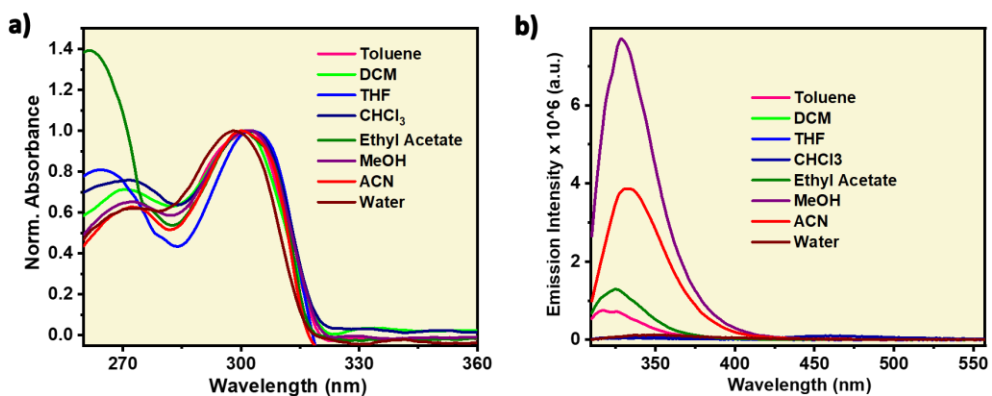


Figure S8: a) Normalized absorption and b) fluorescence emission profiles of monomeric DHI in various solvents

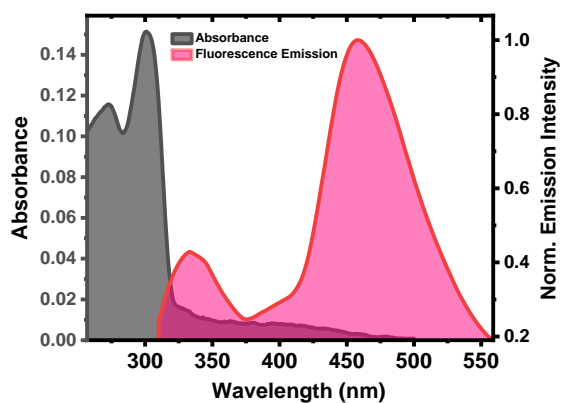


Figure S9: UV-vis absorption (grey) and normalized fluorescence emission (red) profiles of monomeric DHI in CHCl₃.

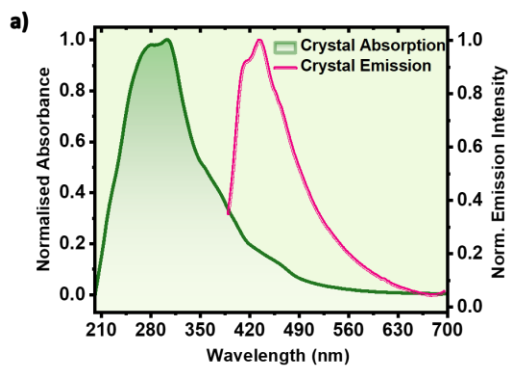


Figure S10: Normalized absorption and fluorescence emission profiles for DHI crystal.

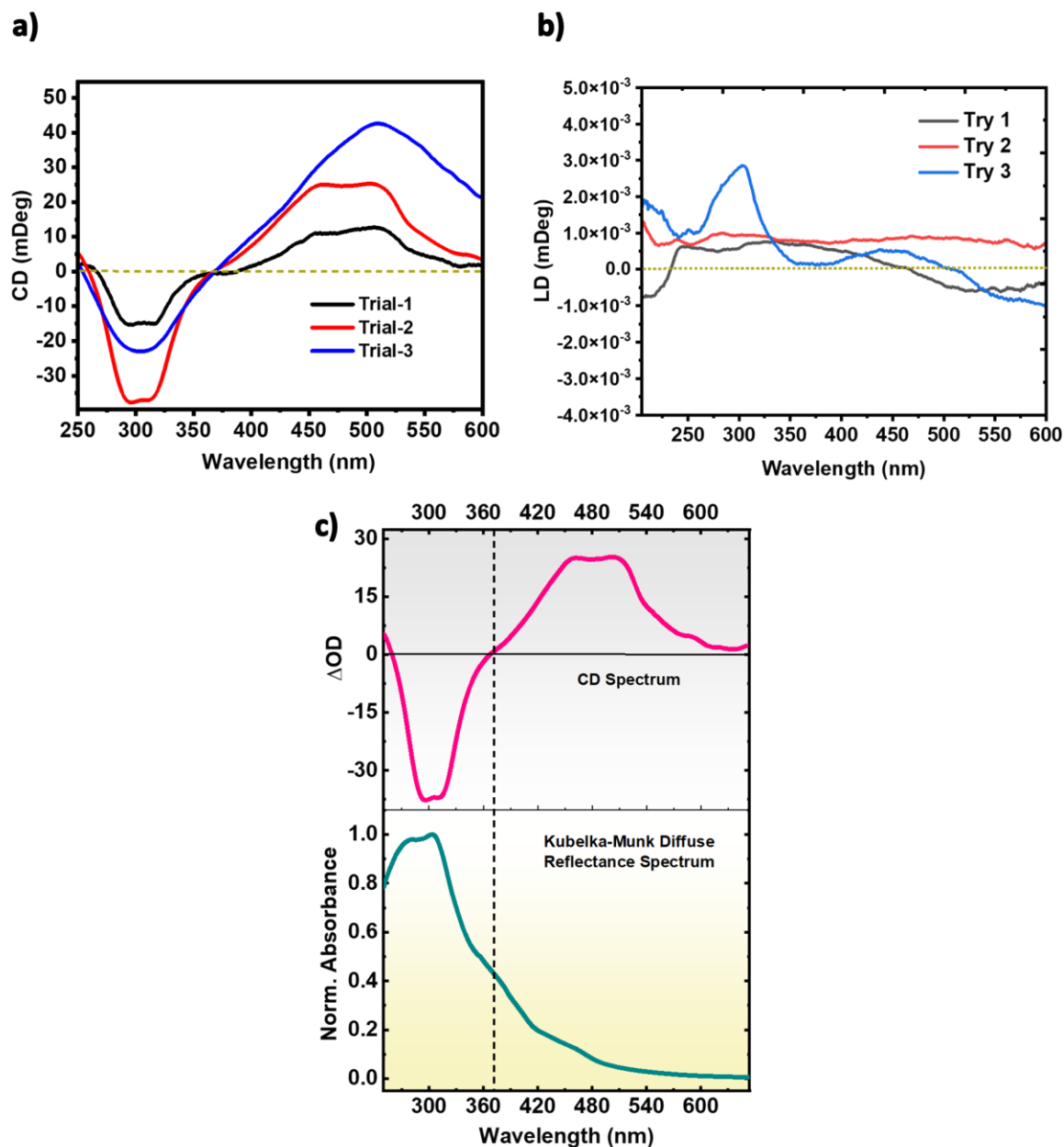
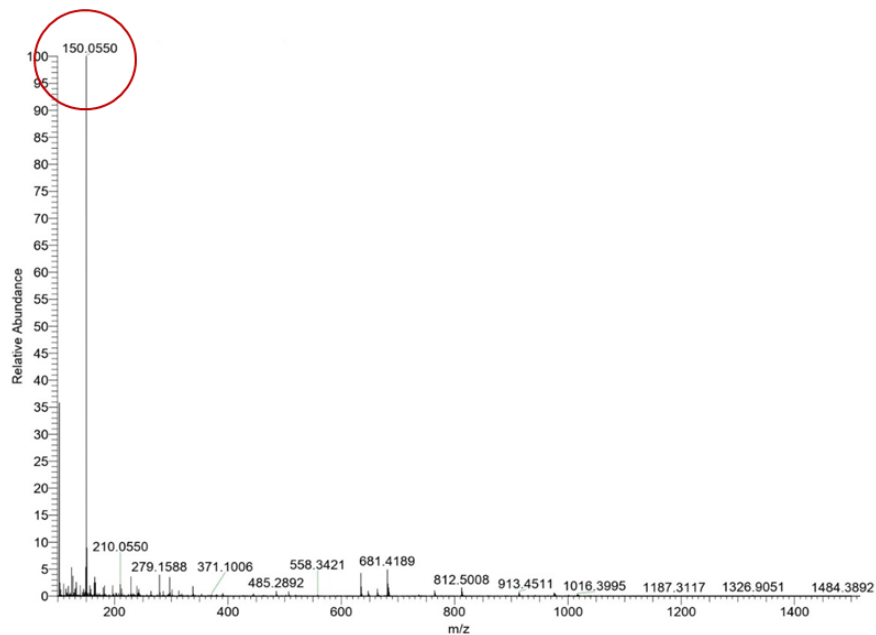
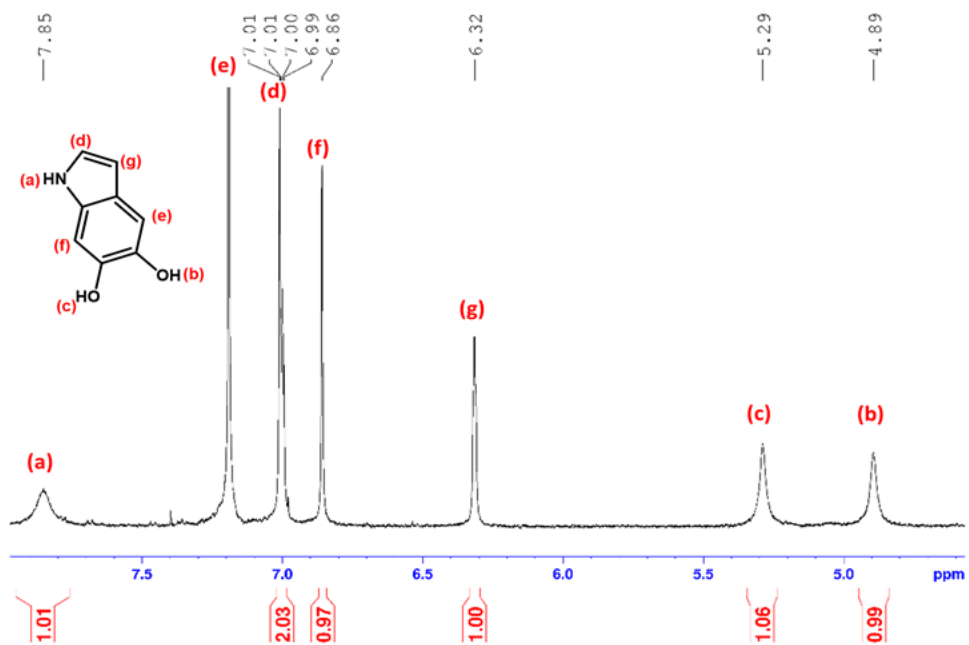


Figure S11: Shows the (a) concurrent CD and (b) LD spectra obtained for the bulk DHI crystal collected on different days, each with freshly crystallized samples at varied concentration ratio of sample:KBr. c) Kubelka-Munk diffuse reflectance spectrum (bottom) and CD spectrum (top) of DHI crystal with the zero crossing at ~ 371 nm.

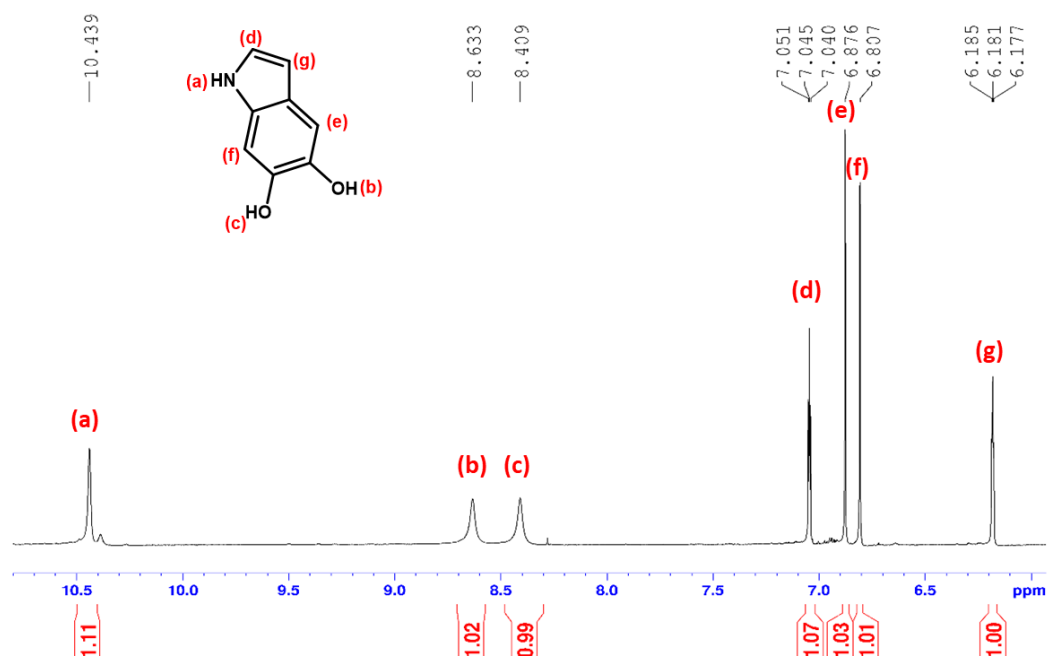
Section E: Appendix-Characterisation Data



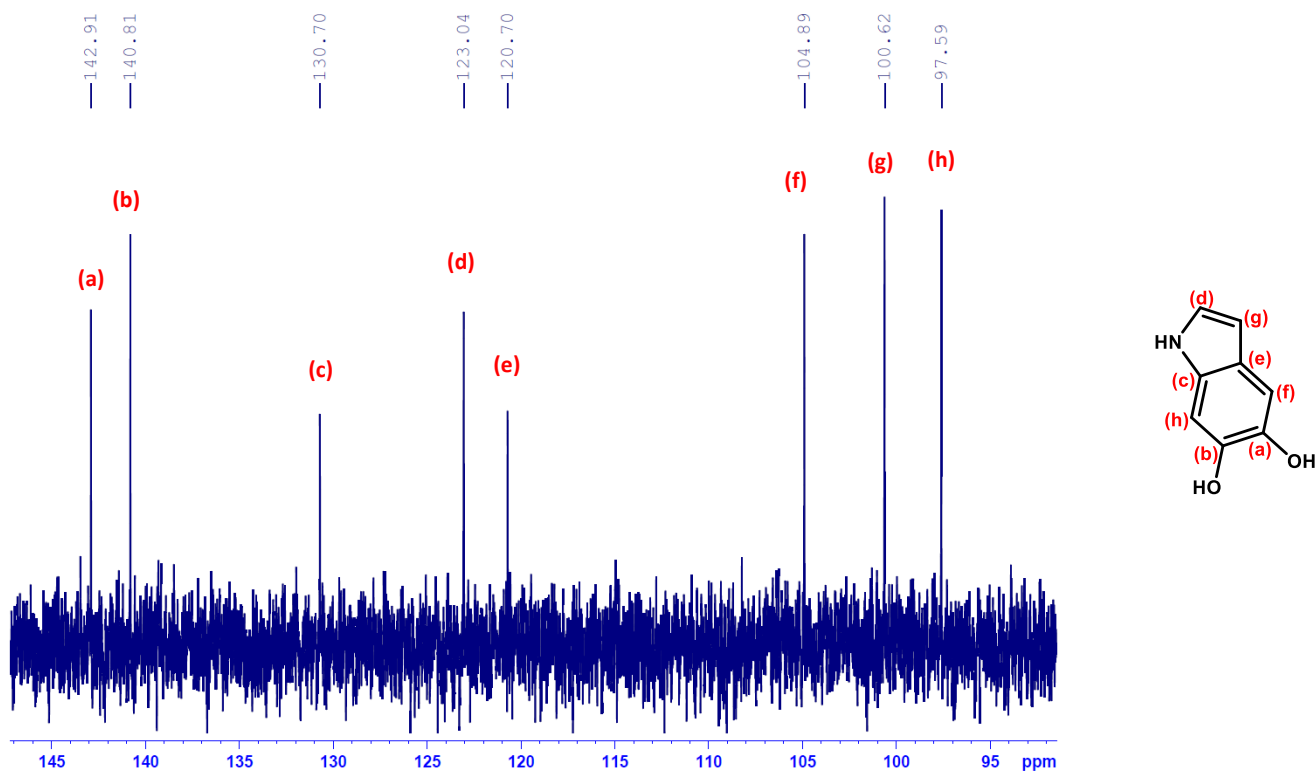
Appendix C1. HRMS Spectrum of DHI monomer



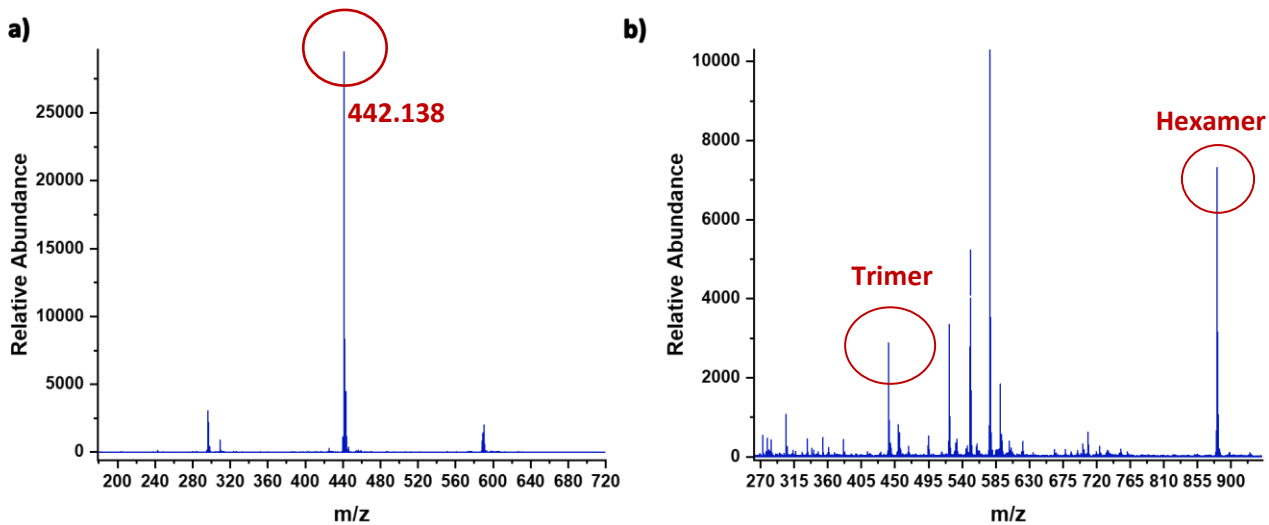
Appendix C2: ¹H-NMR Spectrum of DHI-monomer in CDCl₃.



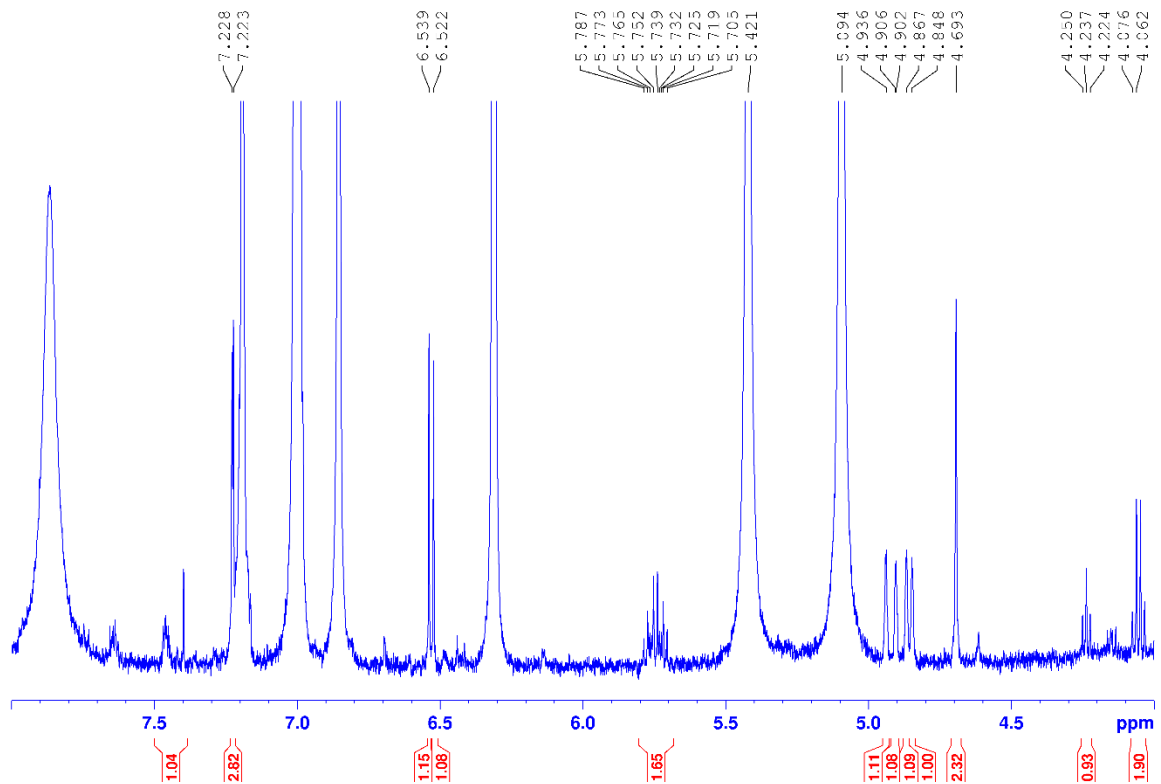
Appendix C3: ¹H-NMR Spectrum of DHI in DMSO-d₆.



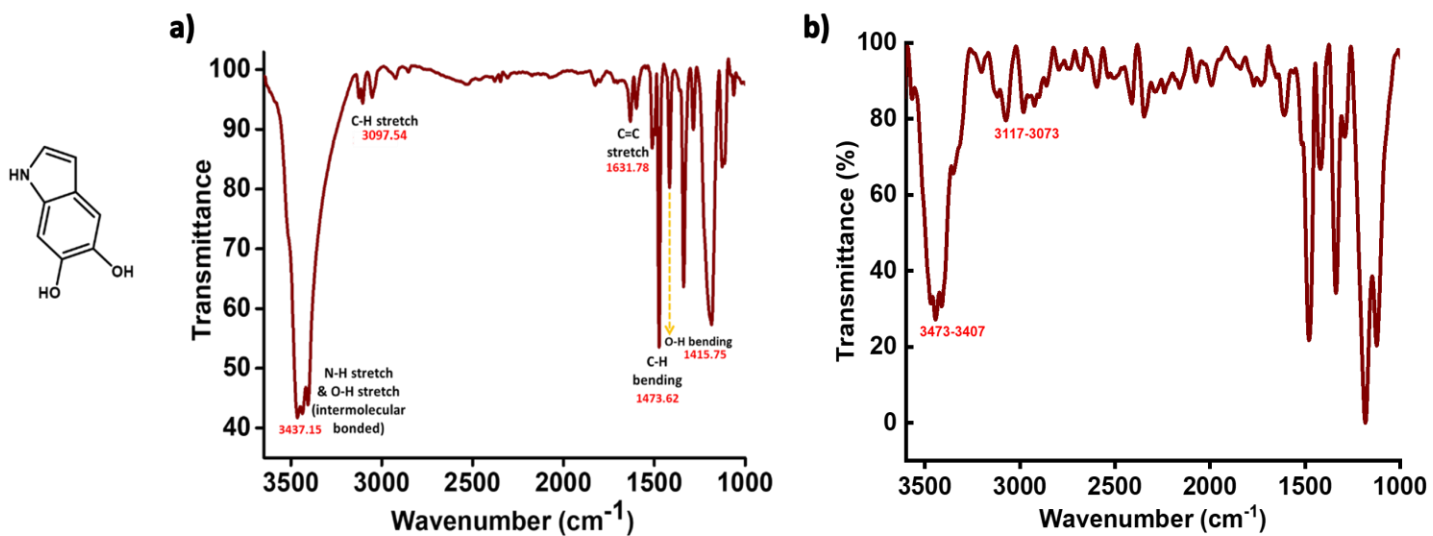
Appendix C4: ¹³C-NMR Spectrum of DHI in DMSO-d₆.



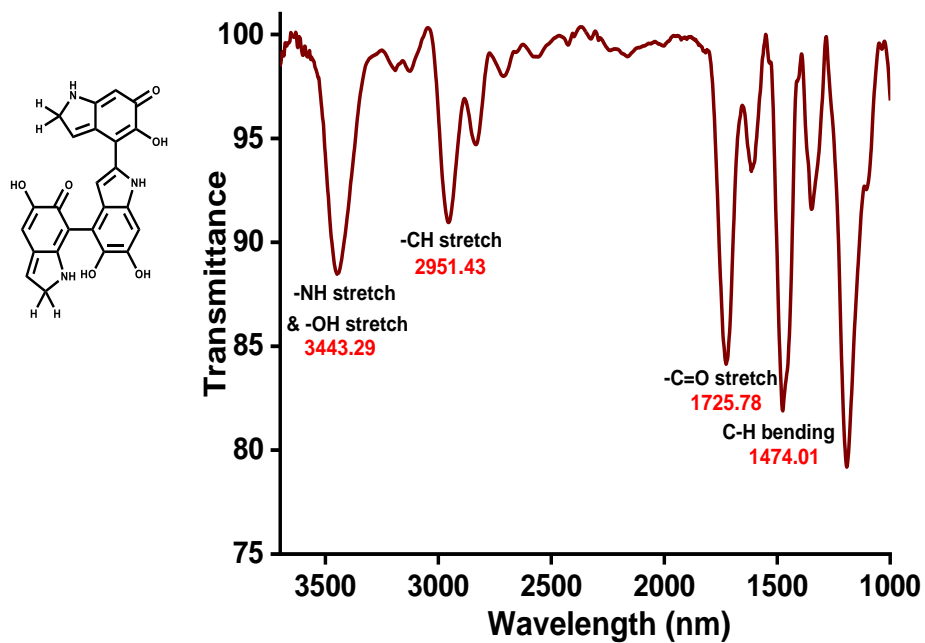
Appendix C5: MALDI-MS Spectra of DHI-oligomer dissolved in **a)** CHCl_3 and **b)** DMSO.



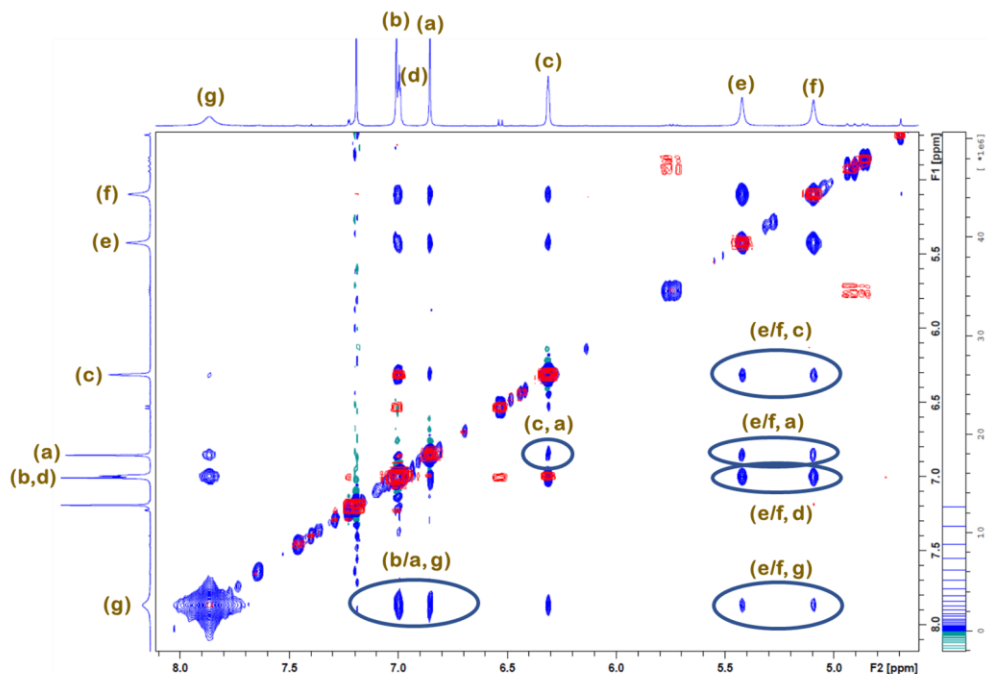
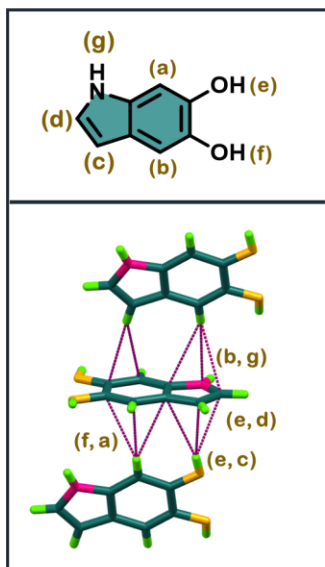
Appendix C6: $^1\text{H-NMR}$ spectrum showing the presence of DHI-T in aggregate concentrations of DHI in CDCl_3 . The 17 protons obtained after proton integration point to a trimer structure as that of DHI-T.



Appendix C7: IR Spectrum of DHI in a) KBr pellet and b) Chloroform solution.



Appendix C8: IR Spectrum of DHI-T in KBr pellet.



Appendix C9: Shows the overlapped 2D ¹H-COSY (red) and -NOESY (blue) NMR spectra of DHI in CDCl₃. The proximal hydrogen atoms having through space interactions are marked and are in line with the obtained crystalline packing motif of DHI crystal.

Section F: REFERENCES

- (1) Wakamatsu, K.; Ito, S. Preparation of Eumelanin-Related Metabolites 5,6-Dihydroxyindole, 5,6-Dihydroxyindole-2-Carboxylic Acid, and Their O-Methyl Derivatives. *Analytical Biochemistry* **1988**, *170* (2), 335–340.
- (2) Sheldrick, G. M. A Short History of *SHELX*. *Acta Crystallographica Section A Foundations of Crystallography* **2008**, *64* (1), 112–122.
- (3) Farrugia, L. J. *WinGX* Suite for Small-Molecule Single-Crystal Crystallography. *Journal of Applied Crystallography* **1999**, *32* (4), 837–838.
- (4) Bruno, I. J.; Cole, J. C.; Edgington, P. R.; Kessler, M.; Macrae, C. F.; McCabe, P.; Pearson, J.; Taylor, R. New Software for Searching the Cambridge Structural Database and Visualizing Crystal Structures. *Acta Crystallographica Section B Structural Science* **2002**, *58* (3), 389–397.
- (5) Gaussian 16, Revision C.01, Frisch, M. J.; Trucks, G. W.; Schlegel, H. B.; Scuseria, G. E.; Robb, M. A.; Cheeseman, J. R.; Scalmani, G.; Barone, V.; Petersson, G. A.; Nakatsuji, H.; Li, X.; Caricato, M.; Marenich, A. V.; Bloino, J.; Janesko, B. G.; Gomperts, R.; Mennucci, B.; Hratchian, H. P.; Ortiz, J. V.; Izmaylov, A. F.; Sonnenberg, J. L.; Williams-Young, D.; Ding, F.; Lipparini, F.; Egidi, F.; Goings, J.; Peng, B.; Petrone, A.; Henderson, T.; Ranasinghe, D.; Zakrzewski, V. G.; Gao, J.; Rega, N.; Zheng, G.; Liang, W.; Hada, M.; Ehara, M.; Toyota, K.; Fukuda, R.; Hasegawa, J.; Ishida, M.; Nakajima, T.; Honda, Y.; Kitao, O.; Nakai, H.; Vreven, T.; Throssell, K.; Montgomery, J. A., Jr.; Peralta, J. E.; Ogliaro, F.; Bearpark, M. J.; Heyd, J. J.; Brothers, E. N.; Kudin, K. N.; Staroverov, V. N.; Keith, T. A.; Kobayashi, R.; Normand, J.; Raghavachari, K.; Rendell, A. P.; Burant, J. C.; Iyengar, S. S.; Tomasi, J.; Cossi, M.; Millam, J. M.; Klene, M.; Adamo, C.; Cammi, R.; Ochterski, J. W.; Martin, R. L.; Morokuma, K.; Farkas, O.; Foresman, J. B.; Fox, D. J. Gaussian, Inc., Wallingford CT, **2016**.
- (6) Bader, R. F. W. A Quantum Theory of Molecular Structure and Its Applications. *Chemical Reviews* **1991**, *91* (5), 893–928.
- (7) Spackman, M. A.; Jayatilaka, D. Hirshfeld Surface Analysis. *CrystEngComm* **2009**, *11* (1), 19–32.
- (8) Plasser, F.; Lischka, H. Analysis of Excitonic and Charge Transfer Interactions from Quantum Chemical Calculations. *Journal of Chemical Theory and Computation* **2012**, *8* (8), 2777–2789.
- (9) Plasser, F. TheoDORE: A Toolbox for a Detailed and Automated Analysis of Electronic Excited State Computations. *The Journal of Chemical Physics* **2020**, *152* (8), 084108.
- (10) Szalewicz, K. Symmetry-Adapted Perturbation Theory of Intermolecular Forces. *WIREs Computational Molecular Science* **2012**, *2* (2), 254–272.